Effects of an Intercalating Agent on the Morphology and Thermal and Flame-Retardant Properties of Low-Density Polyethylene/Layered Double Hydroxide Nanocomposites Prepared by Melt Intercalation

Lei Ye, Qianghua Wu

Key Laboratory of Soft Matter Chemistry (Chinese Academy of Sciences), Department of Polymer Science and Engineering, University of Science and Technology of China, Hefei, Anhui, China 230026

Received 2 March 2010; accepted 13 November 2010
DOI 10.1002/app.33770
Published online 27 July 2011 in Wiley Online Library (wileyonlinelibrary.com).

ABSTRACT: The effects of an intercalating agent on the morphology and thermal and flame-retardant properties of low-density polyethylene (LDPE)/layered double hydroxide (LDH) nanocomposites were studied with Fourier transform infrared spectroscopy, X-ray diffraction, transmission electron microscopy, microscale combustion calorimetry, thermogravimetric analysis, and mechanical property measurements. X-ray diffraction and transmission electron microscopy demonstrated that after intercalation with stearate anion (SA) or dodecyl sulfate anion (DS), organo-LDH could be nanodispersed in an LDPE matrix with exfoliated structures or intercalated structures simultaneously with partially exfoliated structures, respectively, via melt intercalation. However, the unmodified LDH composites yielded only microcomposites. Microscale combustion calorimetry, thermogravimetric analysis, and dynamic Fourier transform infrared spectra showed the following order for the flame-retardant and thermal properties: LDPE/SA-modified LDH > LDPE/DS-modified LDH > LDPE/NO_3-modified LDH > LDPE. The higher performance of the LDPE/LDH nanocomposites with respect to flame retardance and thermal stability could be attributed to the better dispersion state of the LDH layers in the LDPE matrix and the greater hindrance effect of LDH layers on the diffusion of oxygen and volatile products throughout the composite materials when they were exposed to burning or thermal degradation. The tensile strength and elongation at break of the LDPE/LDH nanocomposites decreased to some extent because of the decrease in the crystallinity of the LDPE matrix. A transmittance test showed that the transparency of the exfoliated LDPE/SA-modified LDH nanocomposite was very close to that of neat LDPE. J Appl Polym Sci 123: 316–323, 2012

Key words: blends; modification; nanolayers

INTRODUCTION

In recent years, polymer/layered inorganic nanocomposites (PLNs) have attracted considerable interest because of their dramatically enhanced mechanical performance, thermal stability, flame retardance, and optical properties in comparison with neat polymers or conventional polymer/inorganic composites with microscale inorganic fillers.[1–3] The layered materials in this field mainly include layered silicates, manganese oxides, molybdenum sulfide, titanates, layered phosphates, and layered double hydroxides (LDHs).[3–5] LDHs are considered to constitute a new and emerging class of very favorable layered crystals for the preparation of multifunctional polymer/layered crystal nanocomposites because of their highly tunable properties. They have the general molecular formula $[M^{2+}_{1-x}M^{3+}_{x}(OH)_2]^{x+}A^{n-}_{x/m}nH_2O$, where M^{2+} and M^{3+} are divalent and trivalent metal cations (e.g., Mg^{2+} and Al^{3+}, respectively) and A^{n-} is an interlayer anion (e.g., CO_3^{2-}, NO_3^-, or PO_4^{3-}). Some organic or polymeric anions, such as alkyl carboxylate, polyacrylate, and poly(styrene sulfate), can be intercalated into the interlayers of LDHs by an ion-exchange reaction.[6] However, LDHs are not easy to intercalate or exfoliate[7–9] because LDHs have strong interlayer electrostatic interactions, small gallery spaces, and hydrophilic properties. Therefore, pristine LDHs should be modified with different organic modifiers to alter their surface properties, expand their basal spacing, and facilitate the intercalation of polymers. The resultant organo-LDHs could be applied to the preparation of polymer/LDH nanocomposites via solution intercalation, *in situ* polymerization, and melt intercalation.[10–12] Melt intercalation, which is a nonsolvent, environmentally friendly, and convenient process, is the most important and widely used approach for the preparation of commercial polymers. However, it is always a challenge to obtain a high degree of nanodispersed LDH particles via melt intercalation in comparison with other

Correspondence to: Q. Wu (qhwu@ustc.edu.cn).

technologies (e.g., the solution method) because of the high electrostatic stacking forces between the layers and intercalated anions.[13,14]

Two nanomorphology classes can be observed in PLN nanocomposites: intercalated structures in which the polymer is intercalated in the gallery space between the layers and exfoliated structures in which the delaminated layers are individually dispersed in a continuous polymer matrix. The properties of PLN nanocomposites are often greatly influenced by the morphology. Many articles have reported that PLN nanocomposites with exfoliated structures have properties superior to those of the same PLN nanocomposites with intercalated structures.[15,16] However, some articles have reported that the effects of the nanomorphology on PLN properties differ from the aforementioned results. For example, Samyn et al.[17] prepared a polyamide 6/clay nanocomposite and found that the nanomorphology did not play any significant role in the reduction of the peak heat release rate (PHRR). Giannelis[18] synthesized exfoliated and intercalated poly(ethylene imine)/clay nanocomposites and found that the nanocomposite with an intercalated structure had higher thermal stability than the exfoliated nanocomposite. Samakande et al.[19] observed similar results with polystyrene/clay nanocomposites.

Recently, using LDHs modified by dodecyl sulfate anion (DS) or stearate anion (SA), Liu et al.[20] prepared poly(vinyl chloride)/LDH nanocomposites via a solution-intercalation process. They found that nanocomposites containing SA modified LDH consisting of Mg^{2+} and Al^{3+} cations (MgAl–LDH–SA) had significantly increased thermal stability and dehydrochlorination times in comparison with poly(-vinyl chloride)/DS-modified LDH (LDH–DS) nanocomposites. They concluded from their results that interlayer SAs had an intrinsic ability to absorb HCl. However, they ignored the influence of the morphology on the properties of the nanocomposites.

The aim of this study was to investigate the morphology and flame-retardant and thermal properties of low-density polyethylene (LDPE)/LDH nanocomposites prepared via a melt-intercalation method with LDHs modified by SA or DS. SA has a longer alkyl chain than commonly used DS. Therefore, organic LDHs modified by SA may have larger basal spacing and may be more easily intercalated or exfoliated in a polymer matrix.

EXPERIMENTAL

Materials

The LDPE resin used in this work was obtained from Yanshan Petrochemical Co., Ltd. (Beijing, China). The compatibilizer, maleic anhydride grafted low-density polyethylene (LDPE-*g*-MA) with 0.8 wt % maleic anhydride, was supplied by Shanghai Sunny New Technology Development Co., Ltd. (Shanghai, China). $Mg(NO_3)_2{\cdot}6H_2O$, $Al(NO_3)_3{\cdot}9H_2O$, and sodium stearate were supplied by Shanghai Zhengxing Chemicals No. 1 Plant (Shanghai, China). Sodium dodecyl sulfate and NaOH were obtained from China Medicine (Group) Shanghai Chemical Reagent Corp. (Shanghai, China).

All these chemicals were commercial products and were used as received.

Preparation of the samples

LDH consisting of Mg^{2+} and Al^{3+} cations (MgAl–LDH) was prepared by the coprecipitation method. The pH value of 300-mL aqueous solutions containing $Mg(NO_3)_2{\cdot}6H_2O$ (0.03 mol) and $Al(NO_3)_3{\cdot}9H_2O$ (0.01 mol) with or without an organic modifier (0.01 mol of SA or sodium dodecyl sulfate) was adjusted to approximately 10 with a 1 mol/L NaOH aqueous solution. During the coprecipitation process, the temperature was kept at 70–80°C under flowing N_2 gas with vigorous stirring to exclude CO_2 in the air. The obtained slurry was aged for 3 days at 80°C, filtered, washed with distilled water, and dried at 60°C in an oven for 24 h. This yielded a white powder: SA-modified LDH (LDH–SA), LDH–DS, or NO_3-modified LDH (LDH–NO_3).

The LDPE/LDH–NO_3, LDPE/LDH–DS, and LDPE/LDH–SA samples were prepared by the melt intercalation of LDPE with LDPE-*g*-MA and the corresponding LDH powder with an XSS-300 torsion rheometer (Shanghai Kechuang Machinery Co., Ltd, Shanghai, China) at 140°C for 15 min. The formulations of the various LDPE/LDH samples are summarized in Table I. After blending, the samples were hot-pressed into sheets with a suitable thickness under 10 MPa for 10 min at 140°C.

Measurements

The X-ray diffraction (XRD) patterns were recorded at room temperature (RT) on a X'Pert Pro Super apparatus (Philips Electronics Ltd., Eindhoven, Netherland) with a Cu Kα tube and a nickel filter (wavelength = 0.1542 nm) at a scan rate of 0.0167°/s. The *d*-spacings of the different samples were determined with Bragg's law.

Transmission electron microscopy (TEM) images were obtained on a JEOL 2010 transmission electron microanalyzer (JEOL Ltd, Tokyo, Japan) with an acceleration voltage of 200 kV. The samples were ultramicrotomed with a diamond knife on an LKB Pyramitome to produce 100-nm-thick slices. Then, the slices were transferred from water to a copper grid.

A MCC-2 microscale combustion calorimeter (Govmark Organization Inc., Farmingdale, New York,

TABLE I
Compositions of Various LDPE/LDH Samples

Sample	Composition (phr)				
	LDPE	LDPE-*g*-MA	LDH–NO_3	LDH–DS	LDH–SA
LDPE	95	5	—	—	—
LDPE/LDH–NO_3	95	5	5	—	—
LDPE/LDH–DS	95	5	—	5	—
LDPE/LDH–SA	95	5	—	—	5

United States) was used to investigate the molecular-level flame-retardant properties of the materials according to ASTM D 7309-07. Approximately 5-mg samples were thermally decomposed in an oxygenated environment at a constant heating rate of 1 K/s. Various parameters were measured: the heat release rate (HRR), PHRR, temperature at PHRR (T_{PHRR}), and total heat release (THR). Usually, three measurements were taken for each sample.

The Fourier transform infrared (FTIR) spectra were recorded with a Magna IR 750 spectrometer (Nicolet Instrument Co., Madison, Wisconsin, United States) equipped with a heating device with a temperature controller. The relative concentration of alkyl groups was calculated with the intensity ratio of the related peak height to the maximum height of the 2925-cm^{-1} peak at the thermooxidative degradation temperature.

The transmittance of an LDPE/LDH sheet with a 0.2-mm thickness in the wavelength range of 400–800 nm was recorded on a TU-1901 ultraviolet–visible spectrophotometer (Beijing Purkingji, Beijing, China).

Thermogravimetric analysis (TGA) was performed on a TGA-50H thermal analyzer (Shimadzu Corporation, Kyoto, Japan) at a scan rate of 10°C/min under an air flow rate of 2×10^{-5} m^3/min. Usually, three measurements were taken for each sample.

The mechanical properties were measured with a DCS5000 universal testing machine (Shimadzu Corporation, Kyoto, Japan) at 25 ± 2°C. The crosshead speed was 25 mm/min. The dumbbell-shaped specimens were prepared according to ASTM D 412-87. Usually, five specimens were analyzed to determine the average value for each sample.

RESULTS AND DISCUSSION

Structural characterization of the LDPE/LDH nanocomposites

Figure 1 shows the FTIR spectra of LDH–NO_3, LDH–DS, and LDH–SA samples. All the samples had absorption bands from O—H stretching at approximately 3500 cm^{-1} and a δ (H—OH) vibration at approximately 1630 cm^{-1} arising from the hydroxide layers and interlayer water. The lattice vibration of the *M*—O and O—*M*—O groups (*M* = Mg or Al) was in the 500–800-cm^{-1} region. The absorption bands at 1384 cm^{-1} in the FTIR spectrum of LDH–NO_3 were associated with the asymmetric stretching vibration of the NO_3^- anions.[21] The FTIR spectrum of the LDH–DS sample shows strong absorption at 1226 cm^{-1}, which was assigned to the stretching of RSO_4.[22] The band at 1542 cm^{-1} for the LDH–SA sample may have resulted from the carboxylate asymmetric stretching.[23] In addition, characteristic absorption bands of —CH_3 and —CH_2— groups can be clearly observed at 2800–3000 cm^{-1} in the spectra of the LDH–DS and LDH–SA samples. These results indicate that DS^- or SA^- was intercalated into the layers of LDH.

Figure 2(A) shows the XRD patterns of LDH–NO_3, LDH–DS, and LDH–SA in the 2θ range of 10–60°. The sharp diffraction peaks reveal that the LDHs had typical, well-ordered layer structures. The (003) diffraction peak of LDH–NO_3 at 2θ = 11.2° corresponded to a basal spacing of 0.76 nm. The same diffraction peak was shifted to approximately 2θ = 7° for LDH–DS and to a lower angle for LDH–SA. A weak peak at approximately 11.6° can also be observed in Figure 2(A) for LDH–DS and LDH–SA; this was caused by a small amount of carbonate that formed from CO_2 dissolved in the solution. The contamination of carbonate ions was difficult to avoid, as reported in the literature.[24] Figure 2(B)

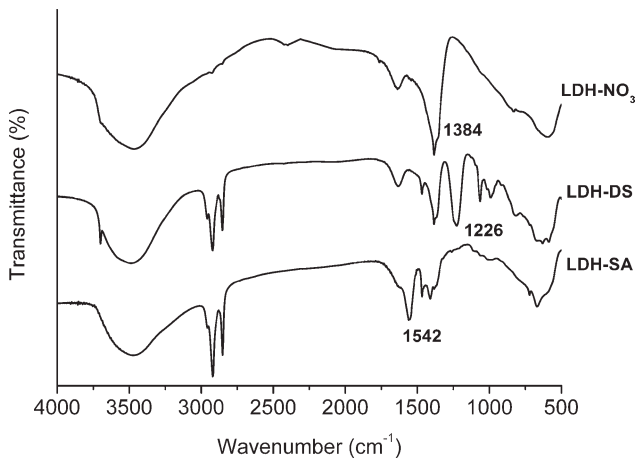

Figure 1 FTIR spectra of LDH–NO_3, LDH–DS, and LDH–SA samples.

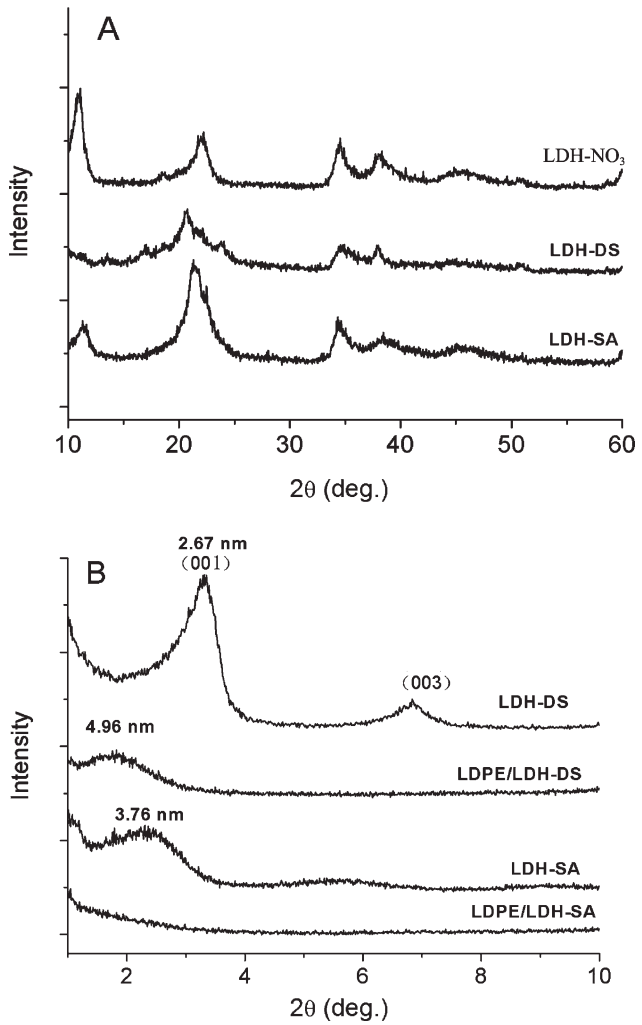

Figure 2 (A) Wide-angle XRD patterns of LDH–NO_3, LDH–DS, and LDH–SA samples and (B) low-angle XRD patterns of LDH–DS, LDH–SA, and LDPE/LDH nanocomposites.

shows the XRD patterns of LDH–DS, LDPE/LDH–DS, LDH–SA, and LDPE/LDH–SA samples in the low-angle range of $2\theta = 1.0$–$10°$. The basal spacings of LDH–DS and LDH–SA were determined to be 2.67 and 3.76 nm from the (001) diffraction peaks at 2θ values of 3.36 and 2.38°, respectively. The increased basal spacing of LDH–DS and LDH–SA indicated that DS^- and SA^- entered the interlayers of LDH. Figure 2(B) also shows that the basal spacing expanded to approximately 4.96 nm, and the (001) diffraction peak became very broad for the LDPE/LDH–DS sample. This indicated that the interlayers of LDH–DS were intercalated by LDPE chains and partially exfoliated in the LDPE matrix during melt intercalation.[25] However, the (001) diffraction peak of the LDPE/LDH–SA sample disappeared, and this indicated that LDH–SA was completely exfoliated in the LDPE matrix.

The microstructure of LDPE/LDH–NO_3, LDPE/LDH–DS, and LDPE/LDH–SA samples was further studied with TEM. Figure 3 presents TEM images of LDPE/LDH–NO_3, LDPE/LDH–DS, and LDPE/LDH–SA samples. Large and unevenly dispersed LDH aggregation with a thickness greater than 500 nm was observed [Fig. 3(A,B)]. This may have been due to the strong attraction force of the LDH–NO_3 layers, which made LDPE/LDH–NO_3 difficult to intercalate or exfoliate in the LDPE matrix. However, LDH layers with intercalated structures (shown by the white arrows) and a few exfoliated LDH layers (shown by the black arrows) could be observed [Fig. 3(C,D), respectively]. The results indicate that the dispersion state of LDH in the LDPE/LDH–DS sample was better than that in LDPE/LDH–NO_3. Figure 3(E,F) shows that the LDH layers were exfoliated and dispersed in a disordered fashion in the LDPE matrix for the LDPE/LDH–SA nanocomposites. The lateral sizes of the exfoliated LDH layers were calculated to be approximately 100–200 nm.

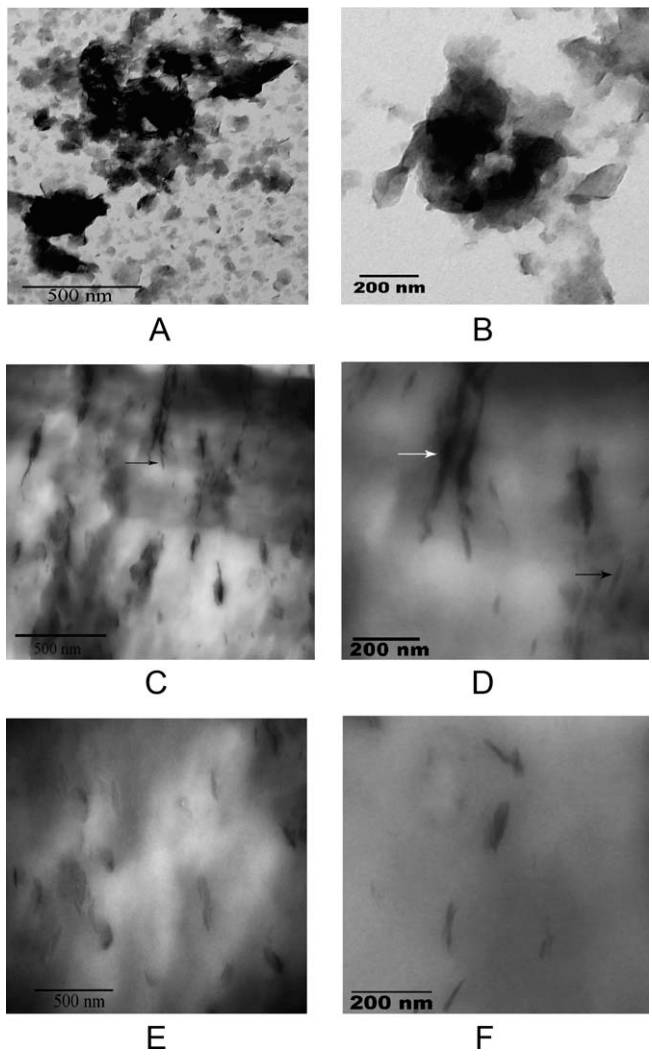

Figure 3 TEM images at different magnifications (500 and 200 nm) of various LDPE/LDH samples: (A,B) 5 phr LDH–NO_3, (C,D) 5 phr LDH–DS, and (E,F) 5 phr LDH–SA.

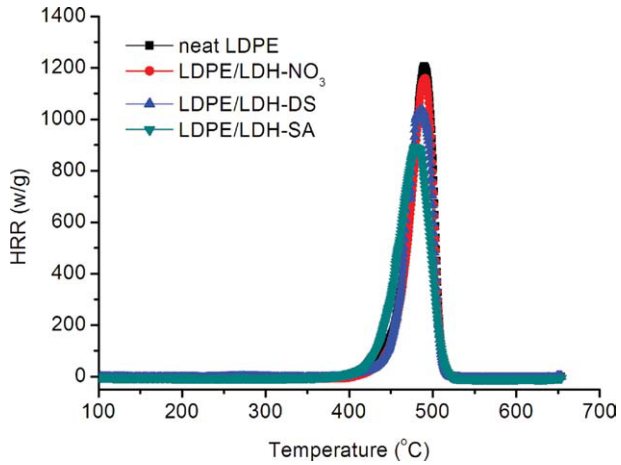

Figure 4 HRR curves of neat LDPE and various LDPE/LDH samples. [Color figure can be viewed in the online issue, which is available at wileyonlinelibrary.com.]

These TEM data were in good agreement with the XRD data, which provided evidence that an organo-LDH intercalated with DS or SA could be significantly nanodispersed in an LDPE matrix with intercalated structures simultaneously with partially exfoliated structures or exfoliated structures via melt intercalation, respectively. The better dispersion of LDH–SA versus LDH–DS in the LDPE matrix may have been due to the larger basal spacing of LDH–SA versus LDH–DS, which made it easier for LDPE chains to penetrate the interlayers of LDH during melt intercalation.[26]

Flame-retardant properties of the LDPE/LDH nanocomposites

Microscale combustion calorimetry (MCC) has become one of the most effective bench-scale methods for investigating the combustion properties of polymer materials. MCC uses oxygen consumption calorimetry to measure the rate and amount of heat. The heat is produced by the complete combustion of fuel gases generated during the controlled pyrolysis of a milligram-sized sample.[27] HRR is the most important parameter in evaluating the fire hazard of materials.

Figure 4 presents HRR curves of neat LDPE, LDPE/LDH–NO_3, LDPE/LDH–DS, and LDPE/LDH–SA samples. The corresponding combustion data are presented in Table II. Table II shows that

TABLE II
Part Data Recorded in the MCC Experiments

Sample	PHRR (w/g)	PHRR reduction with respect to LDPE (%)	THR (kJ/g)	T_{PHRR} (°C)
LDPE	1230	—	43.3	491
LDPE/LDH–NO_3	1170	5	41.5	488
LDPE/LDH–DS	1051	14.5	40.4	483
LDPE/LDH–SA	898	27	40.1	481

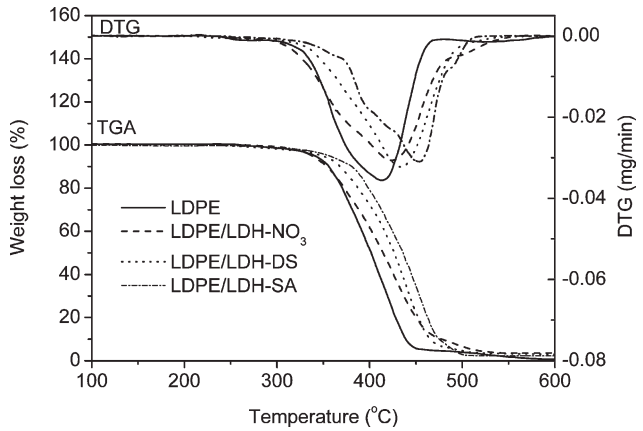

Figure 5 TGA and DTG curves of LDPE and various LDPE/LDH samples.

PHRR of neat LDPE was 1230 w/g. However, PHRR decreased sharply with the addition of LDH. The PHRR values were 1170, 1051, and 898 w/g for the LDPE/LDH–NO_3, LDPE/LDH–DS, and LDPE/LDH–SA samples, respectively, and they were reduced by 5, 14.5, and 27%, respectively, in comparison with the value for neat LDPE. THR showed the same trend as PHRR for the LDPE/LDH samples. The exfoliated LDPE/LDH–SA nanocomposite had the lowest THR value among all the samples, as shown in Table II. These results indicate that nanoscale-dispersed LDH layers (especially exfoliated LDH layers) can greatly enhance the flame-retardant properties of polymeric materials. However, the addition of LDH decreased T_{PHRR} for the LDPE/LDH samples, and this may have been caused by the initial thermal decomposition of the interlayer anions, as reported in the literature.[28]

Thermooxidation stability of the LDPE/LDH nanocomposites

Figure 5 illustrates the TGA and differential thermogravimetry (DTG) curves of neat LDPE, LDPE/LDH–NO_3, LDPE/LDH–DS, and LDPE/LDH–SA samples. The LDPE/LDH samples had higher thermal stability than neat LDPE in the range of 300–550°C. Detailed analysis data are given in Table III. The initial decomposition temperatures at a 5 wt % weight loss for LDPE/LDH–NO_3, LDPE/LDH–DS, and LDPE/LDH–SA samples were 326, 347, and 348°C, respectively, which were 1, 22, and 23°C higher than the initial decomposition temperature at a 5 wt % weight loss for neat LDPE (325°C). The temperatures of the maximum mass-loss rate were 423, 435, and 449°C, respectively, and were 9, 21, and 35°C higher than the temperature of the maximum mass-loss rate for neat LDPE (414°C). When the 50% weight loss was selected as a point of comparison, the thermal decomposition temperatures for

TABLE III
Thermal Degradation Temperatures at Different Stages and Residues Obtained from TGA for LDPE and Various LDPE/LDH Samples

Sample	T_{onset} (°C)[a]	T_{max} (°C)[b]	$T_{0.5}$ (°C)[c]
LDPE	325	414	401
LDPE/LDH–NO_3	326	423	413
LDPE/LDH–DS	347	435	426
LDPE/LDH–SA	348	449	436

[a] Thermal degradation temperature at a 5 wt % weight loss.
[b] Thermal degradation temperature at the maximum loss rate of the degradation stage.
[c] Thermal degradation temperature at a 50 wt % weight loss.

neat LDPE, LDPE/LDH–NO_3, LDPE/LDH–DS, and LDPE/LDH–SA samples were determined to be 401, 413, 426, and 436°C, respectively. Obviously, exfoliated LDH was better for improving the thermal stability of LDPE than microdispersed or intercalated LDH.

Figure 6 shows dynamic FTIR spectra obtained from the thermooxidative degradation of neat LDPE, LDPE/LDH–NO_3, LDPE/LDH–DS, and LDPE/LDH–SA samples in the condensed phase with the pyrolysis temperature increasing from RT to 500°C. Notably, all the samples showed peaks at 2925, 2845, 1455, and 1346 cm^{-1}. The peak at 2925 cm^{-1} was assigned to the asymmetric stretching vibration of the CH_2 group, whereas the peak at 2845 cm^{-1} was assigned to the symmetric stretching vibration of the CH_2 group. The peak at 1455 cm^{-1} was assigned to the asymmetric deformation vibration of the CH_2 group, whereas the peak at 1375 cm^{-1} was assigned to the symmetric deformation vibration of the CH_2 group.[29,30] The intensities of all these peaks for all the samples decreased rapidly with the pyrolysis temperature increasing because of the thermooxidative degradation of the polyethylene main chains. Figure 7 shows the changes in the relative peak intensities at 2925 cm^{-1} with the pyrolysis temperature for neat LDPE, LDPE/LDH–NO_3, LDPE/LDH–DS, and LDPE/LDH–SA samples. The thermooxidation rates of all the samples were almost the same from RT to approximately 200°C. However, when the temperature was higher than 200°C, the

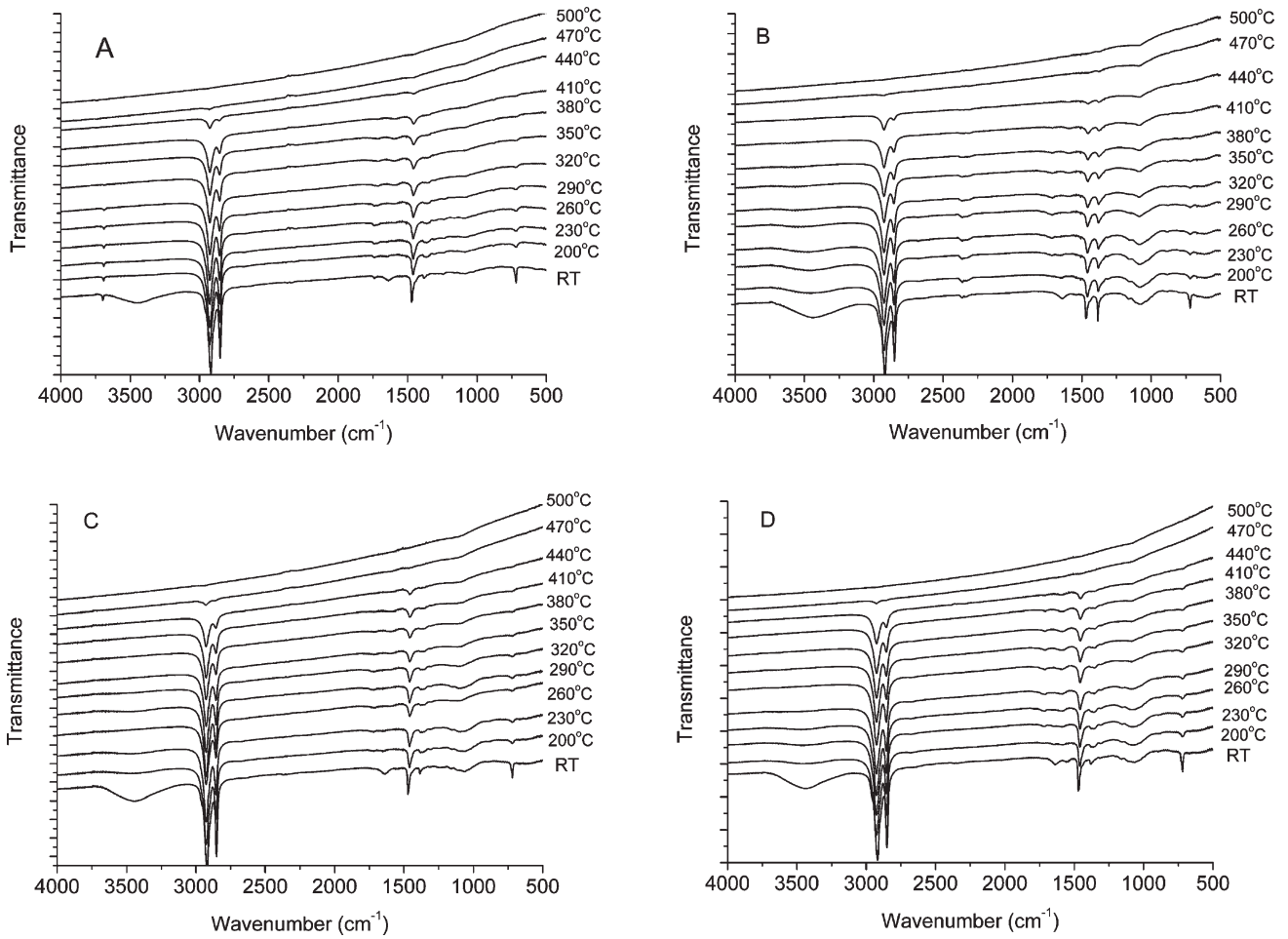

Figure 6 Dynamic FTIR spectra at different thermooxidative temperatures: (A) neat LDPE, (B) LDPE/LDH–NO_3, (C) LDPE/LDH–DS, and (D) LDPE/LDH–SA.

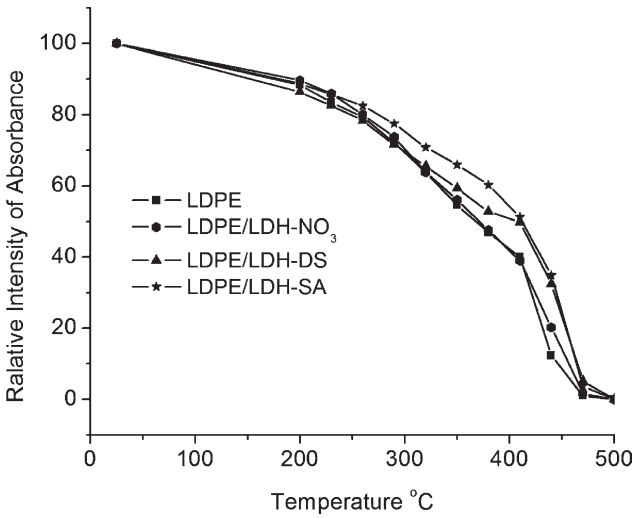

Figure 7 Relative peak intensities of the absorbance at 2925 cm^{-1} assigned to the —CH_2— or —CH_3 asymmetric vibration in LDPE and its nanocomposites.

relative peak intensities of the LDPE/LDH samples at 2925 cm^{-1} were much higher than those of neat LDPE. LDPE/LDH–SA had the slowest thermal pyrolysis rate, as shown in Figure 7. This apparent improvement of the thermal stability for the exfoliated LDPE/LDH nanocomposites can be explained as follows: at the high temperature, the exfoliated LDH layers acted as heat insulators and mass transport barriers and played a key role in preventing further degradation and weight loss of the polymer.

Mechanical properties of the LDPE/LDH nanocomposites

The mechanical properties of LDPE and three kinds of LDPE/LDH samples are listed in Table IV. All the LDPE/LDH samples had decreased values of the tensile strength and elongation at break in comparison with the neat LDPE resin. The mechanical properties of a filled polymer material depend on two principal factors: the crystallinity of the polymer and the reinforcement effect of the fillers.[31] Figure 8 shows the XRD patterns of neat LDPE, LDPE/LDH–NO_3, LDPE/LDH–DS, and LDPE/LDH–SA samples in the 2θ range of 5–60°. The intensities of the (110) and (200) diffraction peaks of LDPE decreased after the addition

TABLE IV
Mechanical Properties and Crystallinity of LDPE and Various LDPE/LDH Samples

Sample	Tensile strength (MPa)	Elongation at break (%)	Crystallinity (%)
LDPE	14.8	873	45.3
LDPE/LDH–NO_3	8.5	171	38.6
LDPE/LDH–DS	11.4	648	36.5
LDPE/LDH–SA	11.8	678	35.3

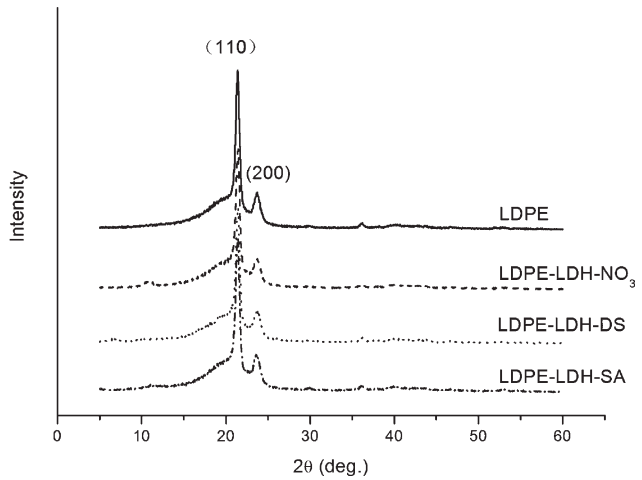

Figure 8 XRD patterns of LDPE and its nanocomposites in the 2θ range of 5–60°.

of LDH, and this indicated a decrease in the crystallinity of the LDPE matrix. The crystallinity of the neat LDPE matrix was analyzed on the basis of the XRD diffraction patterns with the following expression:[32,33]

$$\chi_c = (I_c^{110} + I_c^{200})/(I_a + I_c^{110} + I_c^{200})$$

where χ_c is the crystallinity of the neat LDPE matrix and I_a and I_c^{hlk} are the areas under the amorphous halo and the *hlk* reflections, respectively. Table IV lists the crystallinity values of neat LDPE, LDPE/LDH–NO_3, LDPE/LDH–DS, and LDPE/LDH–SA samples. The crystallinity values of LDPE/LDH–NO_3, LDPE/LDH–DS, and LDPE/LDH–SA samples were measured to be 38.6, 36.5, and 35.3%, respectively; they were much lower than the value for the neat LDPE (45.3%). The decrease in the crystallinity upon the addition of LDH may be attributed to the higher interfacial area and adhesion between the LDPE matrix and LDHs (especially for the exfoliated LDH layers), which reduced the mobility of crystallizable chain segments. The same phenomenon has been mentioned in the literature.[28] Therefore, the decreased mechanical properties of the LDPE/LDH samples could be attributed to the decreased crystallinity of the LDPE matrix. However, the LDPE/LDH nanocomposites showed better mechanical performance (higher tensile strength and elongation at break) than the LDPE/LDH–NO_3 composite. The increase in the tensile strength could be related to the reinforcement brought by the very stiff, high-aspect-ratio nanoclays, which interacted across a very large total interfacial area with the matrix.[34]

Optical properties of the LDPE/LDH nanocomposites

Figure 9 shows the transparency of LDPE and various LDPE/LDH samples. The transmittance of

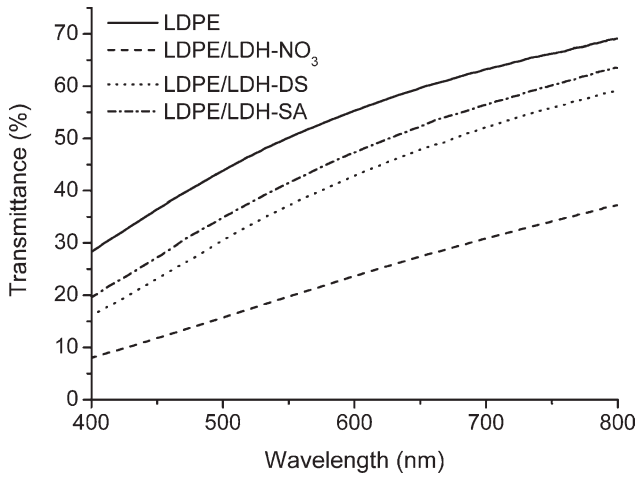

Figure 9 Transmittance of 0.2-mm-thick LDPE and various LDPE/LDH samples.

various LDPE/LDH samples was lower than that of neat LDPE because of the strong scattering of the LDH particles. However, the transmittance of the LDPE/LDH nanocomposites was better than that of the LDPE/LDH–NO_3 sample. The different transmittances of various LDPE/LDH samples could be attributed to the different dispersion states of the LDH layers in the LDPE matrix. LDH–NO_3 agglomerated in the LDPE matrix and deflected or reflected the light greatly. However, the layers of LDH–DS and LDH–SA were intercalated or exfoliated in the LDPE matrix. The single LDH layer did not deflect or reflect the light because its size was smaller than the wavelength of light. Therefore, the scattering effect of LDH particles in the LDPE/LDH nanocomposites was reduced, and the LDPE/LDH nanocomposites showed higher transmittance. As shown in Figure 9, the transmittance of the LDPE/LDH–SA nanocomposite was very close to the transmittance of neat LDPE. These results indicated that the optical clarity remained high when LDH was exfoliated in the polymer matrix.

CONCLUSIONS

LDPE/LDH nanocomposites were successfully prepared via a melt-intercalation process with organically modified LDH. The XRD and TEM results showed that the LDPE/LDH–DS sample had intercalated structures simultaneously with partially exfoliated structures, and the LDPE/LDH–SA sample had exfoliated structures. This may have been due to the larger basal spacing of LDH–SA versus LDH–DS. The MCC data demonstrated that the exfoliated LDH layers significantly reduced the HRR and PHRR values of the nanocomposites. The TGA and dynamic FTIR results showed that the exfoliated LDPE/LDH nanocomposites had higher thermooxidative stability and a much slower thermal oxidation rate than neat LDPE, LDPE/LDH–NO_3 microcomposites, and LDPE/LDH–DS nanocomposites. The mechanical tests showed that the values of the tensile strength and elongation at break for LDPE/LDH decreased to some extent in comparison with neat LDPE because of the decrease in the crystallinity of the LDPE matrix. However, because of the nanoscale dispersion of the LDH layers in the polymer matrix, the LDPE/LDH nanocomposites had better mechanical properties than the LDPE/LDH microcomposites. Moreover, the optical clarity remained high when LDH was exfoliated in the polymer matrix.

References

1. Gilman, J. W. Appl Clay Sci 1999, 15, 31.
2. Decker, L. C.; Zahouily, K.; Keller, L.; Benfarhi, S.; Bendaikha, T.; Baron, J. J Mater Sci 2002, 37, 4813.
3. Alexandre, M.; Dubois, P. Mater Sci Eng Rep 2000, 28, 1.
4. Lagaly, G. Appl Clay Sci 1999, 15, 1.
5. Sinha, R. S.; Okamoto, M. Prog Polym Sci 2003, 28, 1539.
6. Leroux, F.; Basse, J. P. Chem Mater 2001, 13, 3507.
7. Adachi-Pagano, M.; Forano, C.; Besse, J. Chem Commun 2000, 91.
8. Leroux, F.; Adachi-Pagano, M.; Intissar, M.; Chauviere, S.; Forano, C.; Besse, P. J Mater Chem 2001, 11, 105.
9. Hibino, T.; Jones, W. J Mater Chem 2001, 11, 1321.
10. Chen, W.; Feng, L.; Qu, B. J. Chem Mater 2004, 16, 368.
11. Peng, H. D.; Tjiu, W. C.; Shen, L.; Huang, S.; He, C. B.; Liu, T. X. Compos Sci Technol 2009, 69, 991.
12. Lee, W. D.; Im, S. S.; Lim, H. M.; Kim, K. J. Polymer 2006, 47, 1364.
13. Costa, F. R.; Wagenknecht, U.; Heinrich, G. Polym Degrad Stab 2007, 92, 1813.
14. Zammarano, M.; Bellayer, S.; Gilman, J. W.; Franceschi, M.; Beyer, F. L.; Harris, R. H.; Meriani, S. Polymer 2006, 47, 652.
15. Alexandre, M.; Doubois, P. Mater Sci Eng A 2000, 28, 1.
16. Fischer, H. Mater Sci Eng A 2003, 23, 763.
17. Samyn, F.; Bourbigot, S.; Jama, C.; Bellayer, S. Polym Degrad Stab 2008, 93, 2019.
18. Giannelis, P. E. Adv Mater 1996, 8, 29.
19. Samakande, A.; Hartmann, P. C.; Cloete, V.; Sanderson, R. D. Polymer 2007, 48, 1890.
20. Liu, J.; Chen, G. M.; Yang, J. P. Polymer 2008, 49, 3923.
21. Newman, S. P.; Jones, W. J. J Solid State Chem 1999, 148, 26.
22. Samal, R. K.; Sahoo, P. K.; Ray, S. S.; Nayak, S. N. Angew Makromol Chem 1985, 129, 11.
23. Ishioka, T.; Maeda, K.; Watanabe, I.; Kawauchi, S.; Harada, M. Spectrochim Acta A 2000, 56, 1731.
24. Chen, W.; Qu, B. J. Chem Mater 2003, 15, 3208.
25. Du, L. C.; Qu, B. J. J Mater Chem 2006, 16, 1549.
26. Lan, T.; Pinnavaia, T. J. Chem Mater 1994, 6, 2216.
27. Lyon, R. E.; Walters, R. N.; Stoliarov, S. I. Polym Eng Sci 2007, 47, 1501.
28. Chen, W.; Qu, B. J. J Mater Chem 2004, 14, 1705.
29. Xie, R. C.; Hu, K. L. Polym Degrad Stab 2001, 72, 313.
30. Wu, Q.; Qu, B. J. Polym Degrad Stab 2001, 74, 255.
31. Gopakumar, T. G.; Lee, J. A.; Kontopoulou, M.; Parent, J. S. Polymer 2002, 43, 5483.
32. Wirsén, A.; Lindberg, T. K.; Albertsson, A. C. Polymer 1996, 37, 761.
33. Kawaguchi, T.; Ito, T.; Kawai, H.; Keedy, D.; Stein, R. S. Macromolecules 1968, 1, 126.
34. Isitman, N. A.; Kaynak, C. Polym Degrad Stab 2010, 95, 1759.